Optimum Science Journal

Journal homepage: https://optimumscience.org

Original Research Article

Finite Element Modeling and Simulation of Die Quenching 22MnB5 Steel Sheets

Haydar Livatyalı *

Yıldız Technical University, Istanbul, Türkiye

ARTICLE INFO

Received 24 June 2024

Accepted 30 August 2024

Available Online 01 December 2024

Keywords:

Hot stamping

Press hardening

Finite element method

Microstructural transformation

ABSTRACT

Mathematical modeling of heat treatment processes necessitates dealing with inherent complexities such as large material property variations, phase transformations, complex inter-parameter couplings, and boundary conditions. A mathematical framework based on a finite element model capable of predicting temperature history and thus, the evolution of phases during heat treatment of the boron steel 22MnB5 through the inverse use of the CCT diagram was developed. This novel model named the "gridding model" was integrated into the commercial FEA software MSC.Marc® by the user subroutine PlotV. The accuracy of the model was verified by simulating some die-quenching experiments in the literature as well as those that were conducted in the laboratory. Simulation results show that if thermo-mechanical-metallurgical couplings are modeled correctly, the proposed model can predict the temperature history and phase transformations with acceptable accuracy.

To cite this article: Livatyalı, H. (2024). Finite element modeling and simulation of die quenching 22MnB5 steel sheets. *Optimum Science Journal (OPS Journal), 2*, 8-31. http://doi.org/10.5281/zenodo.13857500

1. Introduction

Sheet metal forming of steel alloys is traditionally applied at room temperature. To obtain high-strength structural stampings advanced alloys such as high-strength low-alloy (HSLA), dual-phase (DP), transformation-induced plasticity (TRIP), and twinning-induced plasticity (TWIP) steels have been developed and some variants of these classes of alloys have gained common industrial acceptance and practical applications despite the geometry control problems due to relatively higher springback. The alternative solution, hot stamping is limited to fewer steel alloys and 22MnB5 is the most common one. Hot stamping has gained industrial application in the last twenty years, but computer-aided engineering of process and die design of the hot stamping and press hardening processes lagged

* *Corresponding Author: hlivatya@yildiz.edu.tr*

E-ISSN: 3023-817X

industrial practice that found its way into successful parts via expensive trial-and-error. Nevertheless, academic research and publications also reached a mature level introducing basic experimental data needed for design and proposing alternative modeling and simulation methods.

There are two technical problems in finite element modeling and simulation of hot stamping: One of them is the validation of the process and die design so that the time-consuming costly die tryout process is minimized. Industrially applicable and mature solutions have been introduced for this problem category in the collaboration of academia with commercial finite element software developers. The second problem is the prediction and control (tailoring) of the final mechanical properties of stampings. This problem requires modeling and simulation of phase transformations that take place during deformation in which rapid cooling occurs along with some minor heat generation due to plastic deformation, friction, and phase change. The research community has responded to this problem as well, and some industrially useful methods and tools have been developed. Yet, literature still lacks a computationally simple and fast method.

On the second problem, one of the pioneering studies was published by Akerström and Oldenburg (2006). They proposed a model to predict the austenite decomposition into ferrite, pearlite, bainite, and martensite during arbitrary cooling paths for 22MnB5 boron steel sheets. The model was based on Kirkaldy's rate equations modifying for the austenite stabilization effect from the added boron into account. The model was implemented as a material subroutine in the finite element program LS-DYNA. This publication has been taken as the benchmark reference in this article.

Merklein and Lechler (2006) investigated the thermo-mechanical flow properties of precoated 22MnB5 steel sheets experimentally focusing on time–temperature characteristics. The published test data are useful in numerical modeling of the material's deformation behavior during the hot stamping process; however, does not provide any idea about the final material property distribution by the end of stamping.

Tekkaya et al. (2007) proposed a decoupled model where the thermal and microstructural process is simulated in MSC.Marc and the mechanical process is simulated in the dynamic-explicit code PamStamp. They claimed that decoupling of the thermal and mechanical fields during hot stamping simulation yielded a computation time saving of 80%. They also proposed further simplifications such as mathematical modeling of the temperature and rate-dependent flow curve to save from the cost of simulations. These approaches may be valid in the industry where less accurate but guiding solutions are needed in a short time; however, they deviate from a deeper academic understanding of the complex micro and macro processes that take place during hot stamping and press hardening simultaneously.

Shapiro (2009) presented a methodology for finite element modeling of the continuous press hardening of ultra-high strength steel stampings taking the Numisheet 2008 benchmark BM03 as the reference case. LS-DYNA was used as the modeling medium and thermo-mechanical material property data and boundary condition data were

acquired from the literature. This humbly presented work showing how the final material property distribution after hot stamping may be predicted was an enlightening guide for industrial applications.

Billur et al. (2013) stressed the lack of experience in process and die design in hot stamping which involves press hardening as one of the critical phases in the process, and virtual prototyping is proposed as the solution. The process and die design of a typical automotive B-pillar, which is a very common tailor hot stamped component, was elaborated using finite element modeling and simulations using PamStamp. The goal was to control the die quenching process such that the final distribution of phases and thus mechanical properties on the stamped part is controlled along with the geometric distortions on the part. This work proposed an overall strategy on how to use FEM, however, how the phase transformation was predicted within the code is not discussed.

Zhu et al. (2014) studied the deformed austenite decomposition during stamping and quenching based on the transformation, thermodynamic and kinetic theories and the relationship of final microstructure and mechanical properties was experimentally analyzed. The Vickers hardness and mechanical properties of 22MnB5 steel sheets were predicted by the mixture law. A homogeneous and fine lath martensite microstructure was obtained with a cooling rate of 50℃/s (which is much faster than proposed in the literature as 27-30℃/s) and a pressing time of 8 seconds.

Venturato et al. (2017) elaborated on the effects of austenitization temperature, testing temperature, and strain rate on the mechanical and microstructural properties of 22MnB5 sheet experimentally. They showed that all three factors of the hot stamping process influence the final mechanical properties of the stamped parts because they affect the formation of bainite instead of martensite. Therefore, the decoupling approach proposed by Tekkaya et al. (2017) is most probably an oversimplification in cases where prediction and control of final mechanical properties are critical.

This article elaborates on the approach adopted to model plastic deformation and phase change in die quenching (and hot stamping) of 22MnB5 steel sheets using the finite element method. It is the third publication in a series of papers. In the first article (Kocar & Livatyalı, 2020), the aluminized 22MnB5 sheet was subjected to press-hardening followed by austenitizing, both in a conventional furnace and via the conductive (electric resistance) heating method. After press-hardening was performed using these methods, the microstructural and mechanical characterizations of both specimens were performed using optical microscopy, hardness, tensile strength, and high-speed impact tests. The results showed no significant difference was observed in either the microstructure or mechanical properties concerning the heating method used. Regardless of the heating method, the press-hardening process transformed the ferritic-pearlitic microstructure into mostly martensite and some bainite and caused a substantial increase in hardness and strength at the expense of ductility and impact toughness.

The second article (Kocar & Livatyali, 2021) focuses on the assessment of hot forming limits and post-process properties of the 22MnB5 sheets heated to 950°C using the rapid conductive heating method. An experimental

axisymmetric bulging die set was used in stretch forming tests on rectangular specimens with three different widths until failure using cold dies. The tests showed formability limits, while hardness and microstructure analyses of the formed blanks proved the bainitic-martensitic nature.

The current article presents an improved method to predict the die-quenching of 22MnB5 steel blanks using the static-implicit finite element method and including the effects of phase transformation based on the CCT diagram. An approach initially proposed in (Şimşir & Gür, 2008c) as the gridding technique is used to digitize the CCT diagram of the 22MnB5 steel and it is implemented into FEM. A set of die quenching simulations were conducted based on data from the literature (Akerström & Oldenburg, 2006) to validate the proposed method.

2. Methodology

2.1. Numerical Prediction of Thermo-mechanical Processes

Akerström and Oldenburg (2006) used the dynamic explicit finite element method to simulate the transformation of austenite to ferrite, perlite, bainite, and martensite during random cooling of thin boron steel sheets. Numerical modeling was performed by adhering to Kirkaldy's velocity equations and was made operational by employing a subprogram embedded in the finite element model. Building the necessary equations and creating the model, the quantities and ratios of the phases formed by the transformation of austenite during press hardening were predicted. During the experiments, fine-grain boron alloy steel (SSAB Boron 02) was used. According to the results, the proposed model calculated the ratios of the existing phases correctly with an acceptable margin of error. A high amount of bainite was found in the parts of the sheet in contact with the die with the predicted cooling rate of 170^{o}C/s. The latent heat in the material was found to be extremely important in the model. Otherwise, temperature values, especially in the regions not in contact with the die, may give unexpected results. This affects the quantity and distribution of the phases formed and as a result, both the calculated specific heat and the heat transfer coefficients do not give accurate results.

Heat treatment, particularly quenching, is a multi-physical process in which coherent (interdependent, coupled) physical events such as heat transfer, phase transformations, and forming occur simultaneously. Figure 1 summarizes the interactions and correlations of the physical fields with each other (Şimşir & Gür, 2008b). The analytical solution is not possible due to the coherent and nonlinear nature of the problem. However, various numerical approaches such as finite difference method (FDM), FEM, and finite volume method (FVM) have been proposed to solve the problem. Due to its wide application and easy usage, FEM is considered the most practical method for this purpose (Şimşir & Gür, 2008a).

2.1.1. Modeling of heat transfer

Since the correct prediction of the temperature history will directly affect the phase transformation kinetics and temperature-dependent mechanical properties, it is vital to obtain accurate results from heat treatment simulations.

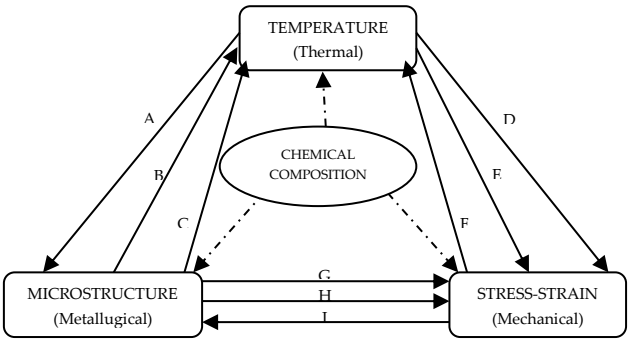

Figure 1. Physical fields and associations in metal forming at elevated temperature (Şimşir & Gür, 2008c).

The accuracy of the temperature history can only be achieved with a deep knowledge of the heat transfer phenomenon. Heat transfer occurs through conduction and phase transformation in the material, with the release of latent heat, and convection and radiation between surfaces. Continuous heat transfer in the material during the heat treatment can be described mathematically with an appropriate form of Fourier's conduction equation (Incropera, F.P. & DeWitt, D. P., 1990). When the latent heat released during phase transformations is included, the equation can be given as follows in its most general form.

$$\boldsymbol{\rho c \frac{\partial T}{\partial t} = div(\lambda \nabla T) + Q} \quad (1)$$

where ρ, c, and λ represent density, specific heat, and thermal conductivity coefficient, respectively. Q represents the latent heat released during phase transformation, and its negligence has a significant side effect on the accuracy of temperature prediction (Denis et al., 1992). The thermal properties of the phase mixture in the internal structure can be determined by the linear mixture rule (2).

$$\boldsymbol{P(T, \xi_k) = \sum_1^N P_k \xi_k} \quad (2)$$

While P represents the average thermal property of the mixture, P_k and ξ_k represent the thermal property of phase k in the phase mixture and the volume ratio of the same phase, respectively (Şimşir & Gür, 2008a). The heat convection boundary condition depending on the surface temperature can be determined by the following equation (3).

$$\boldsymbol{\Phi(T_s, T_\infty) = h(T_s)(T_s - T_\infty)} \quad (3)$$

where Φ is the heat flux at the surface depending on the surface and ambient temperature. $h(Ts)$ is the heat transfer coefficient depending on the surface temperature and T_∞ is the ambient temperature. Similarly, the radiation and isolated surface boundary conditions can be determined by the following equations respectively (4, 5).

$$\boldsymbol{\Phi(T_s, T_\infty) = k_B \zeta (T_s^4, T_\infty^4)} \quad (4)$$

$$\boldsymbol{\Phi = -\lambda \frac{\partial T}{\partial n} = 0} \quad (5)$$

k_B and respectively represent the emissivity of the surface with the Stephan-Boltzman constant. n represents the unit normal vector of the surface (Incropera & DeWitt, 1990).

2.1.2. Modeling of microstructural transformation

Determining the microstructure development during heat treatments requires the generation of numerical models representing the isothermal and anisothermal kinetics of the phase transformations. Anisothermal kinetic models are generally based on isothermal kinetic assumptions and Scheil's additivity principle (Şimşir & Gür, 2008b). The martensitic phase transformation creates microstructure development with diffusion-controlled (ferrite, perlite, and bainite) phase transformations.

Various numerical models have been proposed to represent the isothermal transformation kinetics of diffusion-controlled phase transformations. Many of these models are made up of various modifications based on the same basic principles. According to these isothermal models, the developing phase volume ratio $\xi_k(t)$ of phase k can be determined as a function of time by Equation (6).

$$\boldsymbol{\xi_k = 1 - exp(b_k t^{n_k})} \quad (6)$$

In this equation representing the Johnson-Mehl-Avrami-Kolmogorov (JMAK) kinetic law, b_k and n_k are temperature-dependent kinetic parameters (Askeland, 1993; Şimşir & Gür, 2008b). The JMAK equation can be used in the calculation of phase transformations by developing the following equation when the initial internal structure is a phase mixture (7).

$$\boldsymbol{\xi_k = \xi_k^0 + (\xi_k^{max} - \xi_k^0)(1 - exp(-bt^{n_k}))} \quad (7)$$

k_0 and k_{max} represent the initial and maximum volume ratios and are generally values of 0.05 and 0.95 (Şimşir & Gür, 2008a). This isothermal transformation law can also be used under anisothermal conditions using Scheil's additivity principle. According to Scheil's additive principle, τ (k, T) is the time required for phase *k* to reach *k* phase volume ratio at temperature *T*, and when Scheil sum *S* is equal to one under anisothermal conditions, it will reach the same phase volume ratio (8).

$$\boldsymbol{S = \int_0^t \frac{dt}{\tau(\xi_k, T)} = 1} \quad (8)$$

This rule can be used both in calculating incubation times and determining anisothermal kinetics in phase transformations. As seen in Figure 2, the incubation period under anisothermal conditions can be determined by writing the isothermal incubation time of $\tau_s(Ti)$ instead of $\tau(\xi k, T)$ in the Scheil equation (9).

$$\boldsymbol{S = \sum_{i=1}^{n} \frac{\Delta t_i}{\tau_s(T_i)} \approx 1} \quad (9)$$

In the equation where Δti represents the time step, when S is equal to one, the incubation period is considered complete under anisothermal conditions. After the incubation period is completed, phase development kinetics are calculated as represented in Figure 2. First, an anisothermal imaginary time is determined depending on the phase volume ratio at the end of the previous time step (Şimşir & Gür, 2008b)).

$$\boldsymbol{\tau = \left(-\frac{ln(1-\xi_k(t))}{b_k}\right)^{\frac{1}{n_k}}} \quad (10)$$

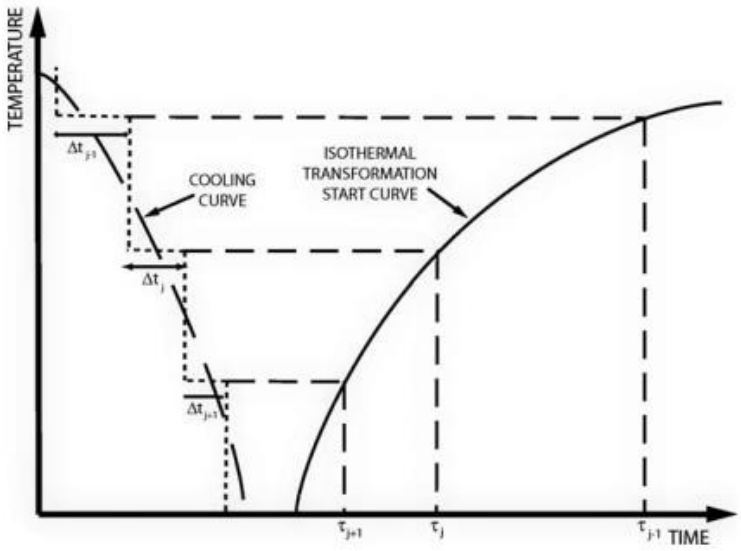

Figure 2. Calculation of anisothermal incubation time with Scheil's additivity principle (Şimşir & Gür, 2008c).

Then, a new imaginary time is obtained by increasing this imaginary time by the time step size *Δt* to calculate the phase volume ratio that will occur under anisothermal conditions in the next time step. Using the imaginary time determined repeatedly in each time step, the phase volume ratio to be newly formed can be determined by the following equation (11).

$$\xi_k^{t+\Delta t} = \xi_k^{max}(\xi_\gamma^t - \xi_k^t)(1 - exp(b_k(\tau - \Delta t)^{n_k})) \quad (11)$$

It is assumed that martensite transformation occurs independently of time below the martensite transformation initiation temperature (M_s). Therefore, conversion kinetics are not affected by the rate of cooling and cannot be determined by Avrami-type kinetic equations. The transformation of austenite to martensite is determined by the following relationship proposed by Koistinen and Marburger (1959).

$$\xi_m = \xi_\gamma(1 - exp(-\Omega(M_s - T))) \quad (12)$$

m and respectively represent the phase volume ratio of martensite and austenite. Ω is a constant value of 0.011 for steels, which is determined with the assumption that M_s will complete 90% martensite conversion under 210ºC (Akerström & Oldenburg, 2006).

2.1.3. An alternative model for microstructural transformation

An improved model was developed that can predict the internal structure development of the materials with given CCT diagrams during the heat treatment process (Kurumahmut, 2009; Şimşir & Gür, 2008b). The details of the gridding model, which is based on the retrospective use of the CCT diagram, are explained below (Figure 3).

The thermo-elastic-plastic model of the hot forming process is based on the constitutive equation determined by the sum of the unit shape changes caused by different physical events such as mechanical stresses, temperature changes and phase transformations (Akerström & Oldenburg, 2006; Belytscko et al., 2000; Koistinen & Marburger, 1959).

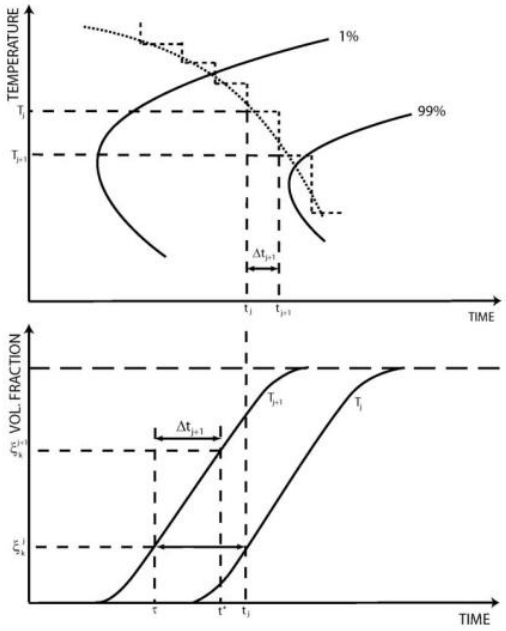

Figure 3. Calculation of anisothermal growth kinetics with JMAK kinetics (Şimşir & Gür, 2008b).

$$\dot{\boldsymbol{\varepsilon}}_{\boldsymbol{ij}} = \dot{\boldsymbol{\varepsilon}}_{\boldsymbol{ij}}{}^{\boldsymbol{e}} + \dot{\boldsymbol{\varepsilon}}_{\boldsymbol{ij}}{}^{\boldsymbol{p}} + \dot{\boldsymbol{\varepsilon}}_{\boldsymbol{ij}}{}^{\boldsymbol{th}} + \dot{\boldsymbol{\varepsilon}}_{\boldsymbol{ij}}{}^{\boldsymbol{pt}} + \dot{\boldsymbol{\varepsilon}}_{\boldsymbol{ij}}{}^{\boldsymbol{tp}} \quad (13)$$

Here, $\dot{\varepsilon}_{ij}, \dot{\varepsilon}_{ij}{}^{e}, \dot{\varepsilon}_{ij}{}^{p}, \dot{\varepsilon}_{ij}{}^{th}, \dot{\varepsilon}_{ij}{}^{pt}, \dot{\varepsilon}_{ij}{}^{tp}$ are the total, elastic, plastic, thermal, and volumetric growth in phase transformation (dilatational phase transformation) and phase transformation plasticity (TRIP) are strain rate tensors.

Hooke's law is used to determine the elastic behavior of the material accepted as linear elastic (Şimşir & Gür, 2008a) and the elastic unit strain is determined by the following equation.

$$\boldsymbol{\varepsilon_{ij}}^{\boldsymbol{e}} = \frac{\mathbf{1}}{\boldsymbol{E}}\left[(\mathbf{1}+\boldsymbol{\nu})\boldsymbol{\sigma_{ij}} - \boldsymbol{\delta_{ij}}\boldsymbol{\nu}\boldsymbol{\sigma_{kk}}\right] \quad (14)$$

Elastic modulus E and Poisson ratio ν depend on temperature and phase volume ratio and are determined by the linear mixing rule. It is called δ_{ij} (Kronecker's delta) (EN ISO 12004-2, 2008) and is given by the following equation.

$$\boldsymbol{\delta_{ij}} = \begin{cases} \mathbf{1}\ \boldsymbol{i} = \boldsymbol{j} \\ \mathbf{0}\ \boldsymbol{i} \neq \boldsymbol{j} \end{cases} \quad (15)$$

σ_{ij} and σ_{kk} represent the stress tensor and the first stress invariant (I_1), respectively (Belytscko et al., 2000). The stress tensor σ_{ij} represents nine stress components perpendicular to the coordinate axes of the stress vectors acting on a small structure whose surface edges are perpendicular to the coordinate axes and are in matrix form.

$$\boldsymbol{\sigma_{ij}} = \begin{vmatrix} \boldsymbol{\sigma_{11}} & \boldsymbol{\sigma_{12}} & \boldsymbol{\sigma_{13}} \\ \boldsymbol{\sigma_{21}} & \boldsymbol{\sigma_{22}} & \boldsymbol{\sigma_{23}} \\ \boldsymbol{\sigma_{31}} & \boldsymbol{\sigma_{32}} & \boldsymbol{\sigma_{33}} \end{vmatrix} \equiv \begin{vmatrix} \boldsymbol{\sigma_{xx}} & \boldsymbol{\sigma_{xy}} & \boldsymbol{\sigma_{xz}} \\ \boldsymbol{\sigma_{yx}} & \boldsymbol{\sigma_{yy}} & \boldsymbol{\sigma_{yz}} \\ \boldsymbol{\sigma_{zx}} & \boldsymbol{\sigma_{zy}} & \boldsymbol{\sigma_{zz}} \end{vmatrix} \quad (16)$$

σ_{kk} is given in the following equation where σ_1, σ_2 and σ_3 represent principal stresses and it is named stress invariance since it is independent of the coordinate system selected in Equation (17).

$$\boldsymbol{\sigma_{kk}} = \boldsymbol{\sigma_1} + \boldsymbol{\sigma_2} + \boldsymbol{\sigma_3} = \boldsymbol{\sigma_{xx}} + \boldsymbol{\sigma_{yy}} + \boldsymbol{\sigma_{zz}} \quad (17)$$

Finally, by taking the derivative of elastic unit strain ε_{ije} with respect to time, the elastic unit strain rate is determined by the following equation (18).

$$\dot{\varepsilon}_{ij}^{e} = \frac{1}{E}\left[-\left(\frac{(1+\nu)\sigma_{ij}-\delta_{ij}\nu\sigma_{kk}}{E}\right)\dot{E} + (\sigma_{ij} - \delta_{ij}\nu\sigma_{kk})\dot{\nu} + (1+\nu)\dot{\sigma}_{ij} - \delta_{ij}\nu\dot{\sigma}_{kk}\right] \quad (18)$$

The thermal strain caused by thermal expansion is determined by the following equation (19).

$$\varepsilon_{ij}^{th} = \sum_{k=1}^{p} \xi_k \int_0^T \alpha_k dT \quad (19)$$

Here, ξ_k represents the volume ratio of the phase *k* and αk represents the temperature-dependent thermal expansion coefficient of the same phase. The thermal unit shape change rate is determined by taking the derivative of the thermal unit shape change according to time (20).

$$\dot{\varepsilon}_{ij}^{th} = \sum_{k=1}^{p} \dot{\xi}_k \int_0^T \alpha_k dT + \xi_k \alpha_k \dot{T} \quad (20)$$

In regions where the unstable austenite turns into ferrite, perlite, bainite, and martensite, there is a volumetric growth due to the difference in density of the main and product phases (Şimşir & Gür, 2008b). The reason for this density difference between phases is that the face-centered cubic (FCC) lattice structure of the austenite phase has a tighter arrangement than the body-centered cubic (BCC) or body-centered tetragonal (BCT) lattice structures of the product phases [LTU]. The volumetric shape change during transformation is reversible and disappears when the product phases turn into the main phase (21).

$$\varepsilon_{ij}^{pt} = \sum_{k=1}^{p} \frac{1}{3}\delta_{ij}\Delta_k\xi_k \quad (21)$$

It represents the structural dilatation that occurs during the transformation of *k* austenite into *k* phase. When the derivative of Equation 21 for time is taken, the volumetric growth unit shape change rate is given as follows (22).

$$\dot{\varepsilon}_{ij}^{pt} = \sum_{k=1}^{p-1} \frac{1}{3}\delta_{ij}\Delta_k\dot{\xi}_k \quad (22)$$

Phase transformation plasticity (TRIP) is the irreversible shape change observed during the solid-state phase transformation that takes place under an external stress lower than the yield strength of the unstable austenite phase. This phenomenon is generally explained by the Magee mechanism and the Greenwood-Johnson mechanism. According to the Magee mechanism, the structure of martensite transformed from austenite in the form of plates creates shear stresses in the internal structure. When no external stress is applied, these plates are oriented randomly and cannot create a stress value that will cause deformation. Under an applied external load, these plates are oriented in the same direction and the internal stresses they create at the micro-scale reach the macro level and cause phase transformation (Akerström & Oldenburg, 2006). The TRIP unit strain rate is determined by the following equation proposed by Leblond (23) (Şimşir & Gür, 2008b).

$$\dot{\varepsilon}_{ij}^{tp} = \frac{3}{2}K_k\dot{\xi}_k(1-\xi_k)S_{ij} \quad (23)$$

where K_k represents the TRIP constant. S_{ij} is the stress deviator (differential stress, stress deviator) and is explained in the next section. The plastic strain of metal materials is independent of the average stress σ_m, also called the hydrostatic component, and depends only on the S_{ij} stress deviator (Akerström & Oldenburg, 2006; Hosford & Caddell, 1993). Average stress σ_m is the arithmetic mean of the principal stresses and is calculated by the following equation (24).

$$\sigma_m = \frac{\sigma_1+\sigma_2+\sigma_3}{3} \quad (24)$$

The stress deviator S_{ij} is in matrix form like the stress tensor σ_{ij} (3x3) and is given by the following equation (25).

$$S_{ij} = \sigma_{ij} - \delta_{ij}\sigma_m \quad (25)$$

The stress deviator S_{ij} in matrix form is as follows (26).

$$\boldsymbol{S_{ij}} = \begin{vmatrix} \boldsymbol{\sigma_{xx} - \sigma_m} & \boldsymbol{\sigma_{xy}} & \boldsymbol{\sigma_{xz}} \\ \boldsymbol{\sigma_{yx}} & \boldsymbol{\sigma_{yy} - \sigma_m} & \boldsymbol{\sigma_{yz}} \\ \boldsymbol{\sigma_{zx}} & \boldsymbol{\sigma_{zy}} & \boldsymbol{\sigma_{zz} - \sigma_m} \end{vmatrix} \equiv \begin{vmatrix} \boldsymbol{\sigma_1 - \sigma_m} & \boldsymbol{0} & \boldsymbol{0} \\ \boldsymbol{0} & \boldsymbol{\sigma_2 - \sigma_m} & \boldsymbol{0} \\ \boldsymbol{0} & \boldsymbol{0} & \boldsymbol{\sigma_3 - \sigma_m} \end{vmatrix} \quad (26)$$

Yield criteria such as Tresca and von Mises are used to understand the conditions under which flow can occur under multi-axial stresses (Hosford & Caddell, 1993). The yield criterion defines a surface that separates the elastic and plastic regions of the materials in the stress space.

According to the von Mises yield criterion, the yield function ψ, which is a function of temperature (T), stress tensor (σ_{ij}), phase volume ratios (k) and the plastic history of the phases (k), is used (Akerström & Oldenburg, 2006) and is determined by the following equation when phase transformations are considered (27).

$$\boldsymbol{\psi(T, \sigma_{ij}, \xi_k, \kappa_k) = F(\sigma_{ij}) - (\sigma_f(T, \xi_k, \kappa_k))^2} \quad (27)$$

Here σ_f represents the variable yield stress. $F(\sigma_{ij})$ represents the equivalent (effective) von Mises stress and the stress deviator is given by the following equation (28).

$$\boldsymbol{F(\sigma_{ij}) = \frac{3}{2} S_{ij} S_{ij}} \quad (28)$$

According to the flow theory, plastic strain is perpendicular to the yielding surface ε_{ijp}. This condition called the normality principle, is represented by the following equation (29).

$$\boldsymbol{\dot{\varepsilon}^p_{ij} = d\lambda \frac{\partial \psi}{\partial \sigma_{ij}}} \quad (29)$$

Here, $d\lambda$ is the factor of proportionality and it is the plastic multiplier condition of continuity (Akerström & Oldenburg, 2006) (Şimşir & Gür, 2008a). The plastic multiplier can be determined using the $d\lambda$ consistency condition and indicates that the stress acting during the plastic deformation will fall on the yield surface together with the yield function (30).

$$\boldsymbol{\dot{\psi} = 0} \quad (30)$$

Plastic history loses its continuity in shaping processes involving phase transformations. The plastic deformation accumulated in the austenite phase is partially or completely lost with the transformation of austenite into product phases. Therefore, it is not appropriate to use equivalent strain as the hardening parameter. Instead, a new hardening parameter k defined for each phase should be used (31) (Şimşir & Gür, 2008b).

$$\boldsymbol{\kappa_k(\tau + \Delta\tau) = \int_{\tau=0}^{\tau} \left(d\dot{\varepsilon}^p - \frac{\dot{\xi}_k}{\xi_k} \kappa_k(\tau) \right) d\tau} \quad (31)$$

Using the hardening parameter k, the variable yield stress σ_f in the phase mixture is determined by the following equation (32).

$$\boldsymbol{\sigma_f = \sum_{k=1}^{N} \xi_k \sigma_k^0 + \sum_{k=1}^{N} \xi_k H_k \kappa_k} \quad (32)$$

σ_{k0} and κ_k respectively represent yield strength and hardening modulus of k phase.

2.2. Mathematical Modeling of Phase Transformations

2.2.1. Gridding of the CCT diagram

The mathematical model proposed in (Şimşir & Gür, 2008c) and explicitly explained above is tested on the case in (Akerström & Oldenburg, 2006) as is (Model 1) and also with some improvement (Model 2) explained in the section below. To establish these models, the phase transformation kinetic parameters (JMAK kinetic parameters) of the material whose microstructure development will be examined must be known. The fact that kinetic parameters of 22MnB5 steel were not available and not yet determined by mathematical approaches, created the need to develop an alternative mathematical model that can predict the development of the microstructure in the absence of these parameters. As a result of this need, a new model has been developed that can predict the microstructure formation and development by using the CCT diagram retrospectively in the absence of these parameters.

The gridding model, which is an innovative approach, is based on the prediction of phase volume ratios (ferrite, perlite, bainite, and martensite) forming the internal structure within each grid by dividing the CCT diagram into time-temperature grids. During the simulation, the temperature (T) of each element forming the geometric model in the simulation and the time spent in the simulation (t) are compared with the time-temperature intervals of each grid in the CCT diagram to determine which grid each element falls in the CCT diagram, and volume ratios are assigned to that element. Figure 4 shows the CCT diagram of 22MnB5 steel (A: austenite, M: martensite, F: ferrite, P: perlite, B: bainite) divided into time-temperature grids (32-time X 56 temperature, 1792 grids in total). Horizontal lines determine the temperature of the grids and vertical lines determine the time limits.

Considering the distance from the phase transformation start and end boundary curves of each grid on the CCT diagram, the phase volume ratios to be found in that grid are predicted linearly. It is assumed that there is a phase volume ratio of at least 1% in the initial limit curve and at most 99% in the end limit curve. According to this approach, the phase volume ratio of the sample grid is determined by the following equation (33).

$$\boldsymbol{X = (99 - 1)\frac{a}{b} + 1} \tag{33}$$

$\boldsymbol{X}$ represents the phase volume ratio (1-99%) of any of the phases that make up the microstructure of the sample grid (ferrite, pearlite, bainite and martensite). *a* represents the distance of the sample grid from the phase transformation of that phase to the initial boundary curve, and b represents the total distance between the boundary curves. The distance of a sample grid to the phase transformation starts curve and the transformation end curve is schematically shown in Figure 5 (1% and 99% are the minimum and maximum volume ratios of that phase respectively). while the formulation of Equation 33 is given schematically in Figure 6.

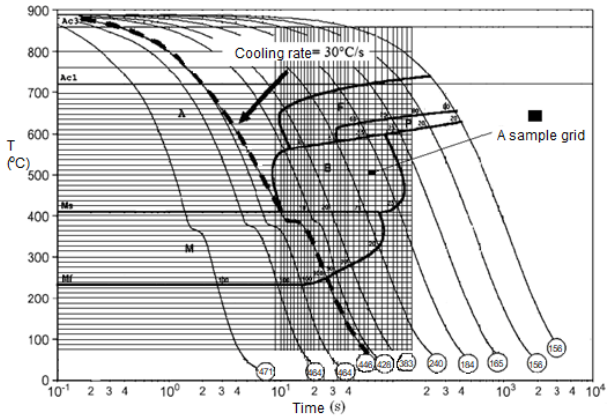

Figure 4. Time-temperature grids as applied to the CCT diagram of 22MnB5 published by (Naderi et al., 2007).

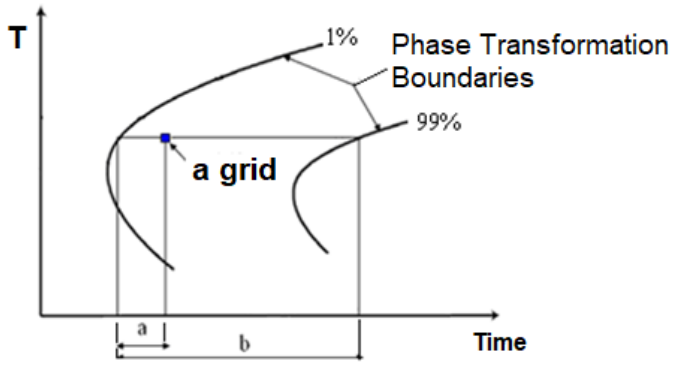

Figure 5. The distance of an example grid from the phase transformation boundary curves (Şimşir & Gür, 2008c).

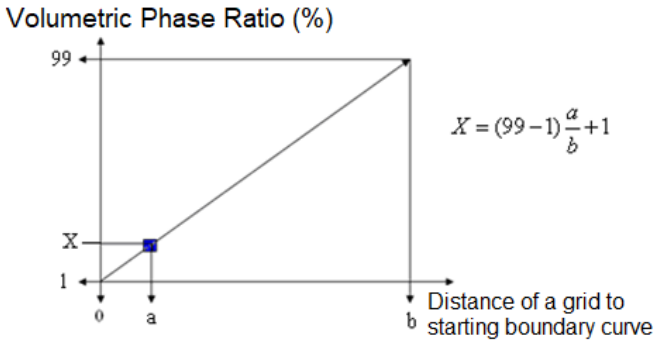

Figure 6. Determination of the phase volume ratio (X) in the grid by reference to the distance of a sample grid from the phase transformation boundary curves.

In the following sections, the details of including the gridding model, which can predict the transformation of the microstructure during hot forming, into the simulation models are explained. Two types of gridding models have been developed based on volume conservation within the grid and volume conservation within the element.

2.2.2. Gridding model 1: Conservation of volume in a grid

The numbers on the cooling curves in Figure 4 are the pre-determined phase volume ratios. For example, curve number 184 shows 60% ferrite, 15% pearlite and 25% bainite. This CCT diagram is divided into time and temperature grids and by referring to these predetermined phase volume ratios and phase transformation boundary

curves on the cooling curves, the phase volume ratios in each grid were predicted using Equation 33 and these values were recorded in the data file (Table 1).

Phase volume ratios in each element (each finite sub-region of the geometric model) in each time step (increment) during the simulation are determined as follows.

- The data in the data file is read and stored in the zeroth time step.
- In the time step to be calculated, it is determined how many grids numbered (i: 1-1792) fall between the time-temperature (z0-z1: s0-s1) boundaries of the current total elapsed time (t) and the current element temperature (T).
- After determining the grid number, phase volume ratios (martensite, ferrite, pearlite, bainite) belonging to that grid are assigned to the relevant element (Figure 7).
- These operations are repeated at each time step during the simulation.

As seen in Figure 7, the elements converging to the cooling curve number 1 first fall into grids with 100% martensite since they have rapid cooling. However, when they reach equilibrium, the temperature is almost unchanged and as time progresses, it is perceived as following a lower-speed cooling curve and falls on grids with a lower martensite volume. Phase ratios first increase and then decrease. Whereas the volume ratio of the product phases transformed from the main phase during cooling should increase or remain constant (principle of irreversibility, force irreversibility).

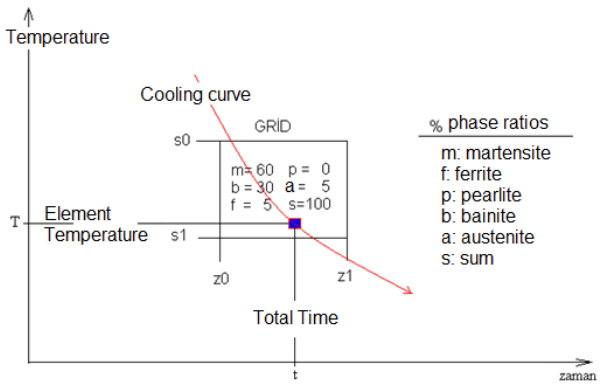

Figure 7. A grid on the CCT Diagram and phase volume ratios of that grid.

The phase volume ratio to be assigned to the element should only be perceived as increasing, that is, it should be in constant comparison with its value in the previous time step. If the volume ratio is lower than the value in the previous time step, the calculation of the volume ratio of the element in question should be stopped (a separate check should be made for each of the martensite, ferrite, perlite and bainite phases) and this should have the highest value during the remaining analysis period.

Table 1. Data belonging to grids on the CCT diagram of 22MnB5.

Grid no (i)	Start Time z0(i) (s)	End Time z1(i) (s)	Start T s0(i) (°C)	End T s1(i) (°C)	% Phase Volume Fractions			
					Martensite mar(i)	Ferrite fer(i)	Pearlite per(i)	Bainite bey(i)
1	0.0	9.0	870.0	800.0	0	0	0	**0**
…	…	…	…	…	…	…	…	**…**
35	0.0	9.0	312.5	300.0	78	0	0	**0**
…	…	…	…	…	…	…	…	**…**
1792	**137.5**	**150.0**	**250.0**	**237.5**	**11**	**55**	**15**	**19**

Considering the constantly increasing or constant values of the phase ratios creates a new problem. It is ensured that the phase volume totals of the elements are preserved as 100% (the sum of martensite, ferrite, pearlite, bainite and austenite volumes equal to 100%) in each grid. However, assigning the volume ratios to the element only as increasing or constant causes the total phase volume of the element to exceed 100%. Because, if the value of one of the phases in the grid where the element is in the previous time step is greater than the value in the new grid, this value is accepted, but since only the values of the other phases of this new grid that are higher than the previous values will be assigned to this element, the total value exceeds 100% (Figure 8).

According to Figure 8, if only grid control is applied to the element, the martensite value will decrease from 80% to 30%. With the assumption that only the increasing values of the phases are assigned to the elements, although there is 30% martensite in the second grid into which the element falls, this value was rejected, and the higher 80% value was assigned to this element. However, as the other phase volume ratios in the second grid are also increasing or constant, the element was assigned exactly, which led to the total phase volume ratio exceeding 100% and reaching 140%.

Taken together, the above problems show that the assumption of volume conservation within the grid is insufficient in modeling the microstructural development. The problems encountered can be eliminated by taking the following measures:

- The conservation of volume in the grid should be abandoned and the conservation of volume in the element should be accepted.
- Each phase volume ratio value of the elements must be compared separately with the values in the previous time step in each time step.

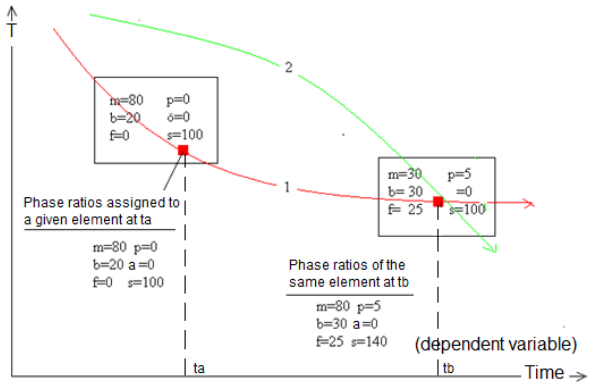

Figure 8. Cooling curve of an element and two grids along this curve.

- Since the transformation of phases can occur only from austenite, the volume of austenite must be constantly controlled, and phase transformations must occur over the last remaining austenite volume.

Considering this information, "Gridding Model 1" should be abandoned and a new model should be developed in which the phase values of the elements in each time step are kept and kept under constant comparison with each other, keeping the phase transformations and the total volume of the phases under control. Phase volume ratio (X) within a grid by taking the distance of it from the phase transformation boundary curves as a reference.

2.2.3. Gridding model 2: Conservation of volume within an element

The most important difference between the second model developed (Kurumahmut, 2009) and the first model is that the phase volume ratio of the martensite transformed depending on the temperature history and the austenite amount is calculated not by reading from the grids in the second method, but by the martensite transformation formula of Koistinen and Marburger (1959) equation. In addition, in this second model, the conservation of volume in the element instead of the volume conservation in the grid was accepted, and the problems such as the decrease in the phases transformed in the element in the first model and the volume growth in the element were eliminated.

The phase transformation flow diagram for determining the microstructure development with the Gridding Model based on the principle of volume conservation within the element is given in Figure 9. Phase volume ratios in each element at each time step during the simulation are determined as follows:

- As mentioned above, the initiation and development of martensite transformation is determined only by temperature control. If the element temperature is equal to or lower than the martensite initiation temperature, it means that the martensite transformation has begun (T <Ms).
- The start of conversion of other phases (ferrite, pearlite, bainite) is controlled over the grids in the CCT diagram. If the phase volume ratio in the grid into which the element falls is greater than zero, it means that the element has entered this phase region in the CCT diagram, and this phase transformation has begun.
- Austenite represents an infinitesimal volume in the structure at each time step in the element.

2.3. Die Quenching Analysis

2.3.1. Modeling of die quenching

In this section, press hardening experiments and simulations presented in the literature are modeled and simulated using the method proposed above, and the results are compared and discussed. For this purpose, the press hardening simulation made in LS-DYNA dynamic-explicit solver used by Akerström and Oldenburg (2006) was repeated using the static-implicit models in the Abaqus® and MSC.Marc® finite element software. The fact that the sheet steel in the related article is the same as the one analyzed (22MnB5 steel), the geometric and the given physical data are sufficient to conduct the simulations and compare the results for the sake of validation.

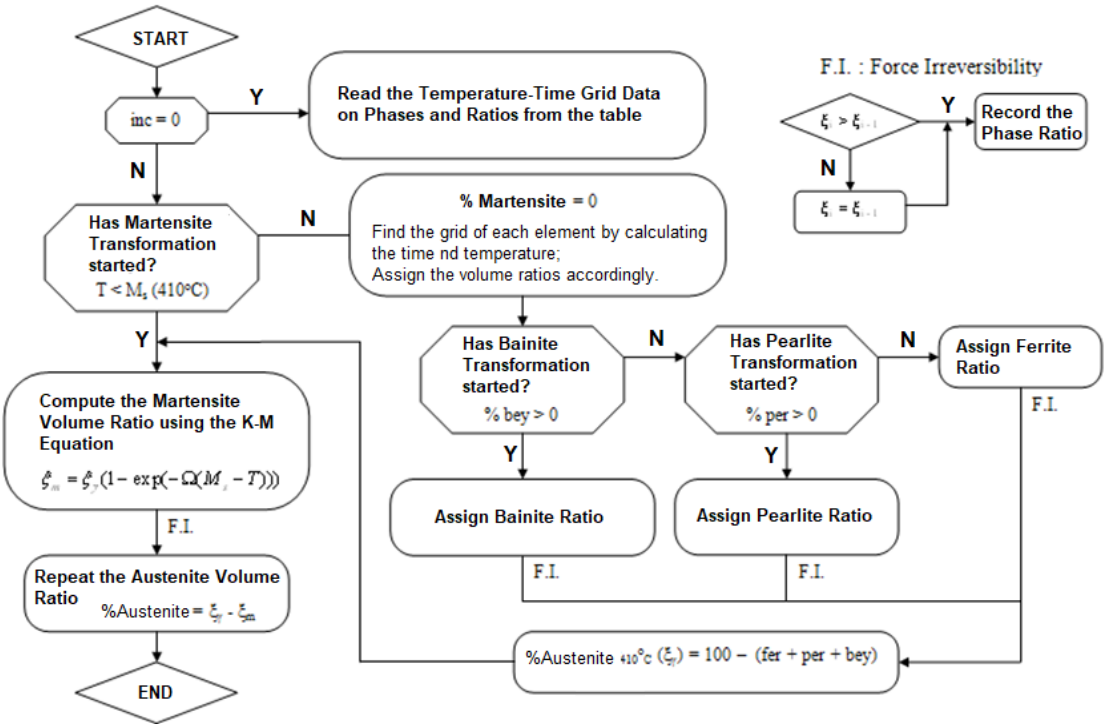

Figure 9. Phase transformation prediction flow diagram

Initially, a static-implicit model using shell elements on the blank and brick elements on the dies was built in Abaqus. The simulations included transient heat transfer from the sheet to the dies; however, the phase transformations were not included. These simulations gave temperature variation in time, but the accuracy was not satisfactory; therefore, the process was re-modeled in MSC.Marc software to simulate the microstructure transformation as a function of time and temperature. The gridding method proposed above was used to predict phase transformations by using the CCT diagram retrospectively. The model was implemented into the MSC.Marc via the user subroutine PlotV.

Figure 10 shows the experimental setup and the test blank with temperature measurement points (Akerström & Oldenburg, 2006). Swedish standard SS2242-02 alloy was used as the tool steel. The specific heat and thermal conductivity coefficients of this steel are given in Table 2 (Şimşir & Gür, 2008b; 2008c). 22MnB5 steel is used as the blank material. and the specific heat and thermal conductivity coefficients of 22MnB5 alloy are given in Table 3 [23]. The changes in specific heat and thermal conductivity coefficients due to phase transformations (updating the thermal properties of the material depending on the volume ratios of the phases transformed in the microstructure) were neglected.

A ¼ geometric model is used due to symmetry, remaining faithful to the reference (Figure 11) (Akerström & Oldenburg, 2006). Both blank and die parts consist of 8-node thermal solid (brick) elements. The initial temperatures of the dies are 27°C while the initial temperature of the blank is 825°C. The heat transfer coefficient between the sheet and die surfaces is given as 6000 W/m^{2}K as the boundary condition. Additional boundary condition values including thermal convection and radiation coefficients from the sheet surfaces not in contact with

the dies are given in Table 4 as a function of temperature (Akerström & Oldenburg, 2006). The ambient temperature is stable at 27ºC.

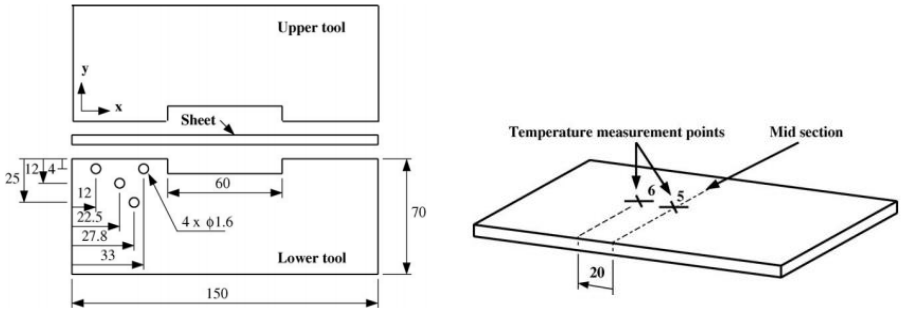

Figure 10. Die quenching experimental set-up and temperature measurement points (Akerström & Oldenburg, 2006).

Table 2. Specific heat and thermal conductivity coefficients of SS2242-02 tool steel (Akerström & Oldenburg, 2006).

T (ºC)	Cp (J/kgºC)	k(W/mºC)
20	460	24.6
400	460	26.2
800	460	27.6

Table 3. Specific heat and thermal conductivity coefficients of 22MnB5 (Akerström & Oldenburg, 2006).

T (ºC)	Cp (J/kgºC)	k(W/mºC)
20	377	46.1
100	477	46.1
200	511	44.8
400	590	39.8
600	741	34.3
800	821	26.4
1000	821	27.2

Table 4. Combined thermal convection and thermal radiation coefficient values (Akerström & Oldenburg, 2006).

T (ºC)	**h_{eff} (W/m^{2}ºC)**
27	0
127	30
227	34
427	36
627	40.4
827	59
1027	92.3

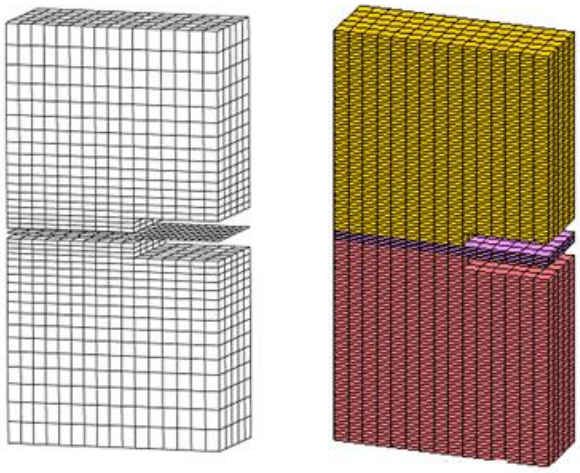

Figure 11. ¼ Symmetrical finite element meshes: (a) by Akerström and Oldenburg (2006) and (b) using MSC.Marc.

2.3.2. Simulation of die quenching

Temperature change with respect to time at two points (P5 and P6) on the blank are compared in Figure 12. Accordingly, the results of the modified MSC.Marc simulations overall compare well with Akerström and Oldenburg's experiments and prediction; however, there are discrepancies in detail. At Points P5 and P6 on the sheet, the temperature values given by the reference (Akerström & Oldenburg, 2006) are higher than the temperature values obtained from Marc's analysis. To put it more accurately, higher cooling rates were predicted in Marc's analysis. The most important reason why the temperature values obtained in the MSC.Marc analysis does not match those in the article is that the thermal properties of the newly formed phases such as specific heat and thermal conductivity coefficient are neglected in the simulation. The values given in Table 3 are the average specific heat and thermal conductivity coefficient values of the sheet material (22MnB5). However, these thermal values vary for each phase and have a significant effect on temperature histories in heat treatment. In addition, the hump seen in the cooling curve around 700°C at Point P5 of (Akerström & Oldenburg, 2006) is missing in our predictions. This is because the latent heat is released with the start of austenite-to-ferrite (from-FCC-to-BCC) conversion.

Figure 13 shows the history of the phase volume ratios predicted by the gridding model at Points P5 and P6 on the sheet. Figure 14 shows the distribution of the martensite volume ratio on the sheet at the end of the die-quenching process. Since the cooling rates obtained in the MSC.Marc simulations are higher than those in (Akerström & Oldenburg, 2006), there are also significant differences between the calculated phase volume ratios, but the proposed model is consistent. Looking at Figure 14, a lower cooling rate is observed at Point P5 in the mid-section of the sheet, as expected, compared to Point P6 20 mm ahead, and as a result, martensite values at Point P5 remain lower than those at Point P6.

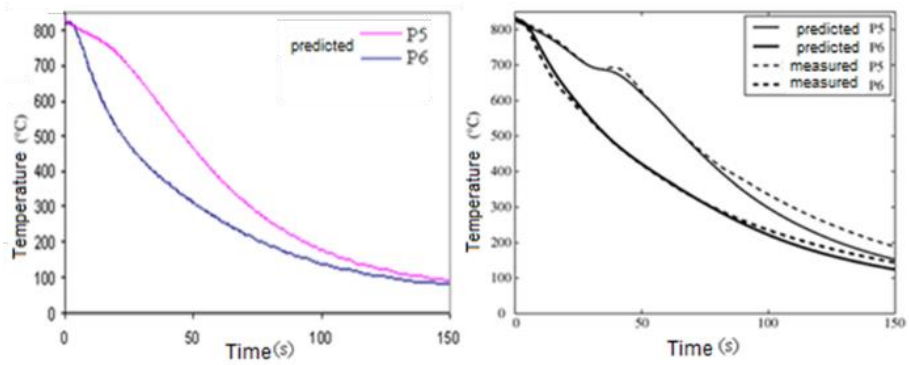

Figure 12. Thermal history of the steel sheet (a) Predicted by the improved static-implicit model in MSC.Marc (b) Akerström and Oldenburg's experiments and simulations (Akerström & Oldenburg, 2006)

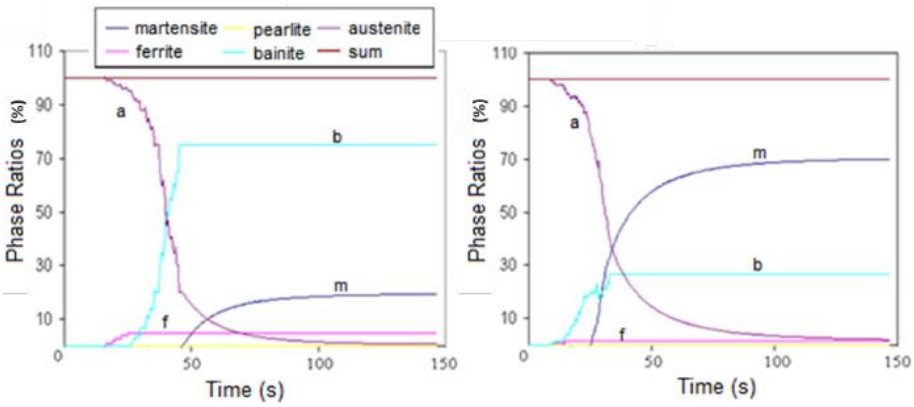

Figure 13: Phase transformations predicted using the gridding model at P6(left) and at P5 (right) (Figure 10).

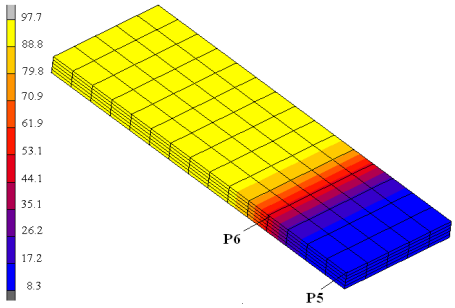

Figure 14: The martensite distribution (volume %) predicted in Marc MSC using the proposed gridding method.

Figure 15 compares final phase distributions along the blank axis predicted using the proposed gridding model and presented by Akerström and Oldenburg (2006). In this diagram, the origin represents the midsection where Point P5 is located and Point P6 is at 20 (mm). The phase variation trends in both studies are similar but there are some discrepancies in values and rates of change. Pearlite predictions are almost the same. The gridding model underpredicted ferrite at P5 as compared to the reference. Bainite reaches 91% at 30 mm from P5 according to Akerström and Oldenburg (2006), but our prediction remains at 72%. The measured hump-like bainite distribution is sharper and more localized, while our distribution is wider and rounder. The same trend repeats at martensite distribution; however, the predicted martensite ratio at a 50 mm distance from P5 (center) agrees very well with the published experimental data. Overall, the finite element simulations with the proposed gridding model predict more

bainite and less martensite means that the transient heat transfer from the blank to the dies is slightly under-predicted compared to the reference.

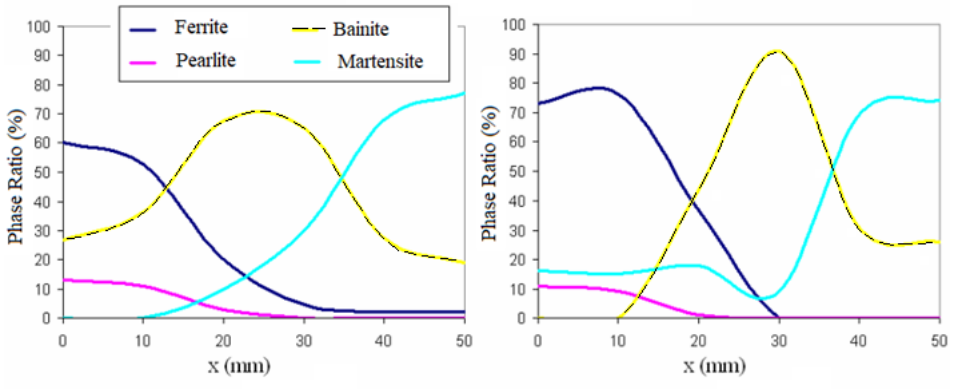

Figure 15. Variation of phase volumetric ration along the X-axis on the blank: As predicted using the improved MSC.Marc implicit model (left) and Akerström and Oldenburg's experiments and simulations (Akerström & Oldenburg, 2006).

3. Results and Discussions

The results obtained from the finite element simulations showed that the proposed model could predict the transformation of the microstructure accurately; however, could not fully reflect the real conditions since the necessary correlations among metallurgical, thermal, and mechanical fields were not completely implemented with some simplifying assumptions. The biggest weakness in the approach is that the physical property couplings are neglected. Most of all, the thermal properties of a metal whose microstructure is constantly changing are implicitly dependent on its temperature history and transformation kinetics. In other words, physical properties including thermal conductivity and specific heat should be computed together with the phase transformation kinetics in each time step during the process. In addition, the latent heat of transformation due to recrystallization (crystal-type conversion from FCC-to-BCC) should also be considered. The cases where it can be neglected can be generalized as the ones with very low Biot numbers. This requires thin blanks, high thermal conductivity, or low (surface) heat transfer coefficient. At high Biot numbers where the surface heat transfer coefficient exceeds the thermal conductivity of the blank, the effect of latent heat can be dramatic. Even the austenite transformed in the center may cause the temperature of the surface to increase up to 100^{o}C.

The thermal properties of the material should be updated continuously through the user subroutines at each time step, considering the individual thermal properties of the transforming phases such as austenite, bainite, ferrite, and pearlite. Below are two sample subroutines that can be used to include thermal property updates based on phase transformations in the simulation model.

- ANKOND subroutine regarding the thermal conductivity coefficient of the phase mixture.
- USPCHT subroutine for specific heat of phase mixture and latent heat of transformation.

Since the thermal properties and latent heat of various phases of the sheet metal (22MnB5) used in the experiment are not available, the average thermal properties of the material were used in the simulation depending on the

temperature, and the subroutines related to the thermal field mentioned above were not included in the simulation model.

Nevertheless, a relatively fast and stable simulation of die quenching was conducted. In the proposed model:

- The cooling rate was slightly under-predicted.
- The latent heat due to ferrite transformation was neglected along with variation of heat capacitance and thermal conductivity due to phases.
- Simulating the press hardening process showed the weaknesses of the model and the critical parameter to control during simulations.
- Therefore, a rougher prediction was achieved.

Accurate thermal properties of the material and heat transfer coefficients are needed. Accurate (element-based) thermal properties may be modeled based on phase volume fractions. Latent heat of phase transformations is also critical because that may affect the temperature change concerning time significantly.

When the presented work was conducted, Li et al. (2021) recent article constructing dilatation curves, phase fraction evolution curves, continuous cooling transformation (CCT), and deformed continuous cooling transformation (DCCT) diagrams were not yet available. The experiments showed that the deformation accelerated the diffusive phase transformation, causing the CCT curves to move in the direction of a shorter incubation time; however, the acceleration of diffusion transformation saturated rapidly as the plastic strain increased. Interestingly, higher strain rates at lower deformation temperatures favored the diffusion phase transformation and the critical cooling rate needed for martensite transformation. The proposed kinetic model implemented into the dynamic-explicit solver of Abaqus reportedly predicted the final phase fraction and hardness of the DCCT specimen, but also the distribution of mechanical properties in the W-channel case study.

10 MPa contact pressure is sufficient for a heat transfer of 3000 $W/m^{2o}C$ and to obtain complete martensite. The phase transformation and predicted microstructure simulated based on the grid model agree well with the experimental results. Simulation of press hardening is a relatively simple case, and thus the proposed phase transformation model is accurate in simulating the die-quenching process.

4. Conclusions

The microstructure formation of the 22MnB5 steel sheets subjected to press hardening was predicted using the static-implicit finite element method modified with a phase transformation model called the gridding method, which is based on the retrospective use of the CCT diagram. This model is integrated into the commercial finite element program MSC.Marc through the user subroutine called PlotV. The accuracy of the model was verified by simulating a case published in the literature.

The proposed method is useful when used for guidance and comparison purposes in future studies. In this context, the main goal of future studies should be to determine the thermal and mechanical properties of the phases that form the microstructure of 22MnB5 steel, and to make and improve the correlations (updating the thermal and mechanical properties coupled with phase transformations) between the metallurgical field and the thermal and mechanical fields in hot forming simulations.

Acknowledgment

This paper is a product of the project 105M178–Forming of Heat Treatable Steel Sheets at Elevated Temperature supported by the Turkish Council of Science and Technology (TUBITAK) and Emre Kurumahmut's master's thesis (Kurumahmut, 2009) supported by the grant. Gratitude also goes to Mr. I. Özcan, Mr. O. Kurumahmut, Prof. M. Demirkol, Prof. H. Çimenoglu, and Prof. M. Baydogan who contributed to the project in various ways and levels. The work was partially presented as an abstract in the proceedings of 13th Int. Conference on the Technology of Plasticity (July 25-30, 2021, Columbus OH USA).

Declaration of Competing Interest and Ethics

The author declares that he has no known competing financial interests or personal relationships that could have appeared to influence the work reported in this paper. This research study complies with research publishing ethics. The scientific and legal responsibility for manuscripts published in OPS Journal belongs to the author.

References

Akerström, P., & Oldenburg, M. (2006). Austenite decomposition during press hardening boron steel—Computer simulation and test. *Journal of Materials Processing Technology*, *174*, 399–406. https://doi.org/10.1016/j.jmatprotec.2006.02.013

Askeland, D. R. (1993). *The science and engineering of materials*. PWS Publishing Company.

Belytscko, T., Liu, W. K., & Moran, B. (2000). *Nonlinear finite elements for continua and structures*. John Wiley & Sons.

Billur, E., Wang, C., Bloor, C., Holecek, M., Porzner, H., & Altan, T. (2013). Advancements in tailored hot stamping simulations: Cooling channel and distortion analyses. *AIP Conference Proceedings*, *1567*(1), 1079–1084. https://doi.org/10.1063/1.4850158

Denis, S., Farias, D., & Simon, A. (1992). Mathematical model coupling phase transformations and temperature evolutions in steels. *ISIJ International*, *32*, 316–325.

EN ISO 12004-2. (2008). *Metallic materials—sheet and strip—determination of forming limit curves—part 2: determination of forming limit curves in the laboratory*. German Institute for Standardization (DIN).

Hosford, W. F., & Caddell, R. M. (1993). *Metal forming: Mechanics and metallurgy*. PTR Prentice Hall.

Incropera, F.P., & DeWitt, D. P. (1990). *Fundamentals of heat and mass transfer*. John Wiley & Sons.

Kocar, O., & Livatyali, H. (2021). Effects of rapid conductive heating and passive cooling with cold dies on hot-forming formability and final mechanical properties of boron steel sheets. *Proceedings of the Institution of*

Mechanical Engineers, Part L: Journal of Materials: Design and Applications, *235*(2), 309–319. https://doi.org/10.1177/1464420720961794

Kocar, O., & Livatyalı, H. (2020). Investigation on the mechanical properties of press-hardened boron steel sheets using the conductive heating technique. *Proceedings of the Institution of Mechanical Engineers, Part L: Journal of Materials: Design and Applications*, *234*(8), 1084–1098. https://doi.org/10.1177/1464420720926532

Koistinen, D. P., & Marburger, R. E. (1959). A general equation prescribing the extent of the austenite-martensite transformations in pure iron-carbon alloys and plain carbon steels. *Acta Metallurgica*, *7*, 59–60.

Kurumahmut, E. (2009). *Finite element analysis o hot stamping 22mnb5 steel sheets* [M.Sc, ITU]. https://tez.yok.gov.tr/UlusalTezMerkezi/tezDetay.jsp?id=C1xPVDjTtS5axiZPPaUPTw&no=wBA9vsrw_x1ftgjKBYeo5Q.

Li, Y., Chen, Y., & Li, S. (2021). Phase transformation testing and modeling for hot stamping of boron steel considering the effect of the prior austenite deformation. *Materials Science and Engineering: A*, *821*, 141447. https://doi.org/10.1016/j.msea.2021.141447

Merklein, M., & Lechler, J. (2006). Investigation of the thermo-mechanical properties of hot stamping steels. *Journal of Materials Processing Technology*, *177*(1–3), 452–455. https://doi.org/10.1016/j.jmatprotec.2006.03.233

Naderi, M., Durrenberger, L., Molinari, A., & Bleck, W. (2007). Constitutive relationships for 22MnB5 boron steel deformed isothermally at high temperatures. *Materials Science and Engineering*, *478*(1-2), 130–139. https://doi.org/10.1016/j.msea.2007.05.094

Shapiro, A. (2009). Finite element modeling of hot stamping. *Steel Research International*, *80*(9), 658–664. https://doi.org/10.2374/SRI08SP065

Şimşir, C., & Gür, C. H. (2008a). 3D FEM simulation of steel quenching and investigation of the effect of asymmetric geometry on residual stress distribution. *Journal of Materials Processing Technology*, *207*, 211–221. https://doi.org/10.1016/j.jmatprotec.2007.12.074

Şimşir, C., & Gür, C. H. (2008b). A FEM based framework for simulation of thermal treatments: Application to steel quenching. *Computational Materials Science*. *44*(2), 588-600. https://doi.org/10.1016/j.commatsci.2008.04.021

Şimşir, C., & Gür, C. H. (2008c). A mathematical framework for simulation of thermal processing of materials: Application to steel quenching. *Turkish Journal of Engineering and Environmental Sciences*, *32*(2), 85-100.

Tekkaya, E. A., Karbasian, H., Homberg, W., & Kleiner, M. (2007). Thermomechanical coupled simulation of hot stamping components for process design. *Production Engineering Research Development*, *1*(1), 85–89. https://doi.org/10.1007/s11740-007-0025-9

Venturato, G., Novella, M., Bruschi, S., Ghiotti, A., & Shivpuri, R. (2017). Effects of phase transformation in hot stamping of 22MnB5 high strength steel. *Procedia Engineering*, *183*, 316–321. https://doi.org/10.1016/j.proeng.2017.04.045

Zhu, L., Gu, Z., Xu, H., Lü, Y., & Chao, J. (2014). Modeling of microstructure evolution in 22MnB5 steel during hot stamping. *Journal of Iron and Steel Research International*, *21*(2), 197–201. https://doi.org/10.1016/S1006-706X(14)60030-3